ENHANCED DIFFUSION BY PROJECTED CURVELET FOR SEGMENTATION WITHOUT GUIDING INFORMATION

[1]Lihong Ma [1]Yu Zhang [2]Hanqing Lu

[1]RICA GDKey Laboratory of Computer Network, Dept. of Electronic Engineering and Communication,
South China University of Technology, Guangzhou, China 510641;
[2] National Lab of Pattern Recognition, Inst. Automation, China Academy of Science, Beijing, China 100080

ABSTRACT

In this paper, we present a new segmentation model, which makes uses of Curvelet's advantages of edge preserving and noise averaging. The model first applies Lorentzian-function based diffusion for stable pixel clustering, and then projects boundaries by Curvelet transform (CT) to enhance edges and modify region smear in diffusion. In particular, we also propose a criterion to seek the appropriate moment for CT enhancement, it is fulfilled by comparing partition results of Lorentzian and Tukey-based functions. If the number of reduced regions between two adjacent segmentation rounds arrives a threshold, CT will be performed to prevent edge disappearing. Experiments show that this significant segmentation is resulted from CT's properties of boundary keeping and denoising, the method is superior to many other PDE approaches.

Index Terms—diffusion model, Curvelet projection, error norm function, revisiting feedback

1. INTRODUCTION

Successful segmentation of objects plays a key role in image analysis, compression and more. However, segmentation is a challenging task, especially when the background is complex and without prior information. Besides the conventional pixel-based or region-based methods, three most popular approaches to image segmentation are Watershed transform, Snakes or active contours and partial differential equations (PDEs) [1]. Morphological Watershed could achieve a good segmentation when object boundaries are close, otherwise over-segmentation will occur [2]. On the other hand, active contours capture the outlines of homogenous regions with a varying penalty term, but many methods of this kind have to assume a priori model for each candidate region. It usually needs a correct initial contour placement, and sometimes a combination of fuzzy clustering and level set methods is also demanded. Even so, it will still result in difficult evolution [3]. In contrast to active contour method, an anisotropic diffusion filter smoothes images primarily along boundaries. Owing to the rapidly decreasing diffusivity of PDE near edges, isotropic pixels in a region are filtered to produce a homogeneous surface, while anisotropic edge points remain stable over a long interval until their gradients reach a low value. Some PDEs, such as Tukey-based function, could develop piecewise constant steady segmentation, but their parametric models have to be trained many times to choose an optimal parameter set, otherwise the diffusion image will converge to isolated cliques like noises [4]. Other PDE solutions are neither unique nor stable. Lorentzian error norm, its weak piecewise solution doesn't exist for the entire interval [5], thus region boundaries begin to smear and areas are blended after some finite time.

To overcome the drawbacks mentioned above, we suggest a new segmentation scheme, in which Curvelet coefficients are projected to an image to emphasize edges and modify the diffusion. It detects object boundaries by integrating over pixels with unknown priori knowledge [6], and strengthens edges to avoid region leakage. Its contributions are mainly to:

(1) It models a segmentation task upon CT boundary enhancement and Lorentzian error norm diffusion. Curvelet projection is applied to stress edges and depress blurring effects while diffusion is marching.

(2) A criterion is developed to determine the timing of CT insertion and diffusion halt. The model combines advantages of sharp stopping characteristic of Tukey-based segmentation and the global region preservation of Lorentzian method.

To demonstrate the validity of our model, we first briefly describe the related diffusion and Curvelet enhancement in Section 2 and 3, and present the suggested segmentation scheme next. Experiments are carried out to create 1) segmentation surface of the original; 2) partitions of the diffused PDE images which are with and without CT enhancement; 3) final results guided by Tukey-based halting condition. The tests show that our method has a superior performance on robust partition than the conventional PDE methods.

2. ERROR NORM BASED DIFFUSION

Anisotropy diffusion produces sharp boundaries of smooth regions. A typical form of anisotropic diffusion for image f is the partial differential equation [7]:

$$\frac{\partial f(x,y,t)}{\partial t} = div(g(\|\nabla f\|)\nabla f) \tag{1}$$

where (x,y) denotes a pixel position in continuous domain and usually replaced by m in discrete occasion. $t=0$ corresponds to initial state, ∇f is a gradient of image f, and $g(.)$ should be a positive monotonous descending function satisfying: (a) $g(\|\nabla f\|)$ tends to be large enough to cause diffusions at positions in a smooth region. (b) $g(\|\nabla f\|)$ will approach zero to retain discontinuity when crossing edges. Discrete form of (1) is expressed by a neighborhood scheme:

$$f_m^{t+1} = f_m^t + \frac{\lambda}{|D_m|}\sum_{n\in D_m} g(\nabla f_{m,n})\nabla f_{m,n} \tag{2}$$

Here t becomes iteration times and λ involves the diffusion rate, $|Dm|$ is pixel numbers of point m's neighborhood Dm.

Different choices of diffusion function ***g(.)*** affect the resulted images. An edge-preserving function based on Tukey's biweight error norm is proposed with its robust estimation $\rho(.)$ and diffusion function ***g(.)*** depicted by (3) and (4):

$$\rho(x,v)=\begin{cases} x^2/v^2 - x^4/v^4 + x^6/v^6 & |x|<v \\ 1/3 & otherwise \end{cases} \quad (3)$$

$$g(x,v)=\begin{cases} (1-(x/v^2))^2, & if \quad |x|\le v \\ 0, & else \end{cases} \quad (4)$$

Though Tukey's functions provide sharper boundaries and improve automatic stopping of diffusion, they are not always converging to stable solutions. Fig.1 is ***g(.)*** of Tukey error norm, it shows that 1) If the parameter sets are not chosen appropriately, diffusion will yield a non-stable solution (as shown in Fig.1(a) and Fig.3(a)). 2) Sometimes edge-stopping will occur as small cliques and finally lead to a noisy image (Fig. 3(b)). 3) Sharper boundaries appear within a region are actually pseudo segmentation (Fig. 3(c)). Fig. 2 is plots of ***g(.)*** related to Lorentzian error norm ρ -function. Its diffusion equation suggested by [7] is:

$$g(x,v) = 1/(K^2 + x^2) \quad (5)$$

Letting $K2 = 2v^2$, we can get the ***g(.)*** with its Lorentzian error norm $\rho(.)$ and diffusion $g(.)$:

$$\rho(x,v) = \log[(2v^2 + x^2)/2v^2] \quad (6)$$

$$g(x,v) = 2/(2v^2 + x^2) \quad (7)$$

Here ***g(.)*** doesn't always descend to zero, thus curves with varying v are quite consistent. If we add constraints on boundaries, Equ. (7) could produce an actual segmentation and prevent region leakage as Fig.3 (d). We could also refer to [8,9] for advances in detail.

3. CURVELET ENHANCEMENT

To overcome the untrue merging, Curvelet transform(CT) and a diffusion halting criterion are introduced in our scheme to emphasizing edges during diffusion marching.

CT is a multi-scale pyramid with Ridgelet analysis on many directions and at each dyadic scale. It involves Radon transform(RT) and Ridgelet computation. The former is a projection with line integrals indexed by angular variable θ, shift variable 1, and $(\theta,t)\in[0,2\pi]\times R$ for image f [6]:

$$Rf(\theta,t)=\int_{-\infty}^{+\infty} f(x_1,x_2)\delta(x_1\cos\theta+x_2\sin\theta-t)dx_1dx_2 \quad (8)$$

here δ is Dirac function. In fact, Ridgelet transform is ***1-D*** wavelet analysis to slices of RT. Coefficients $R_f(a,b,\theta)$ could be calculated with a constant θ and varing 1 s:

$$R_f(a,b,\theta) = \int_{-\infty}^{+\infty} Rf(\theta,t)a^{-1/2}\psi((t-b)/a)dt \quad (9)$$

ψ is a wavelet, $a>0$ and $b\in R$ denote a scale parameter and a translated argument. CT's discrete sketch is [6]:

·Subband decomposition. A standard band-pass filter Δi based on à trous algorithm is applied to decompose subbands:

$$f(x,y) = P_0 f(x,y) + \sum_{j=1}^{J} \Delta_j f(x,y) \quad (10)$$

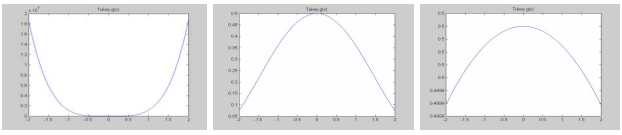

(a) v =0.4 (b) v = 1.6 (c) v =16

Fig.1 Function ***g(.)*** of Tukey biweight estimator.

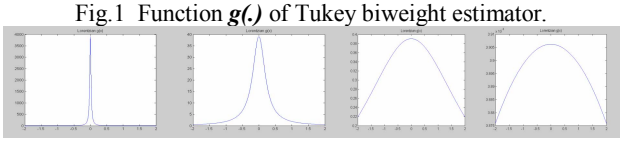

(a) v =0.016 (b) v =0.16 (c) v = 1.6 (d) v = 16

Fig.2 Function ***g(.)*** of Lorentzian estimator.

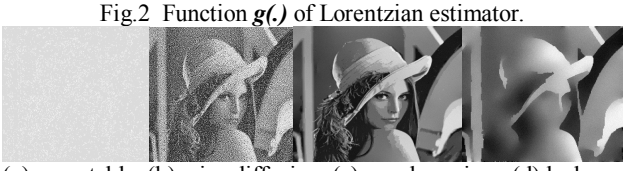

(a) non-stable (b)noisy diffusion (c)pseudo region (d) leakage

Fig.3 Tukey biweight and Lorentzian based Diffusion.

f is decomposed into J subbands: P_0f is the coarse version of f, Δ_{jf} expresses subband details at scale 2^j.

·Smooth Partitioning. Subband Δ_{jf} is partitioned with block side-length B_j in scale j. B_{min} is size of the finest scale, $B_{\min} \sim 2^{-s}$, B_j doubles every other dyadic subband. Thus, if Q is a collection of dyadic squares, Q_{js} are squares of scale j, Δ_{jf} denotes a windowed operation as (11) with sizes as (12):

$$\begin{cases} B_j = 2 * B_{j-1} & if \quad j_{\bmod 2} = 0 \\ B_{j=}B_{j-1} & otherwise \end{cases} \quad (11)$$

$$\Delta_{jf} \mapsto (wQ\Delta_{jf})\ Q\in Q_j \quad (12)$$

. Renormalization and local Ridgelet transform. Each block in a subband is renormalized to unit scale by a transport operator TQ to obtain a dilated function GQ (as (13)). Then Ridgelet transform is performed as defined in (10) and (11).

$$GQ= (TQ)^{-1}(wQ\Delta_{jf})\ Q\in Q_j \quad (13)$$

CT derives object boundaries which are not obvious at pixel level but clear by projection integrating, thus its enhancement to weak edge is well-adapted to boundary preserving. Besides, Curvelet enhancement could be easily realized via multiplying coefficients $w_{j,k}$ at scale j and position k $(k=(x,y))$ [6]. In our work, we use this advantage for the integrity of an object.

4. CRITERION FOR CURVELET INSERTION AND DIFFUSION HALTING

We evaluate the appropriate timing for CT and halting by combining and comparing the segmentation results of two kinds of diffusion, one is Tukey-based, which is sharp stopping but vulnerable to noise, the other is Lorentzian-based, which is stable but easy to region leakage after a long-term diffusion. Since Lorentzian-based region fusion is evolved gradually, we just need to evaluate the moment every 30-iterations (a partition round) by comparing the region numbers of segmentations. If the change count between two adjacent round arrives a threshold, CT will be introduced to prevent edge disappearing. This evaluation includes 3 steps:

1) Initialization of region counters $N^{(0)}_{Lorentzian}$, $N^{(0)}_{Tukey}$ **and initial segmentation result** S_0**.** Here the subscripts Lorentzian and Tukey denote the corresponding diffusions respectively.

2) Homogeneous region propagation. The propagation is implemented by Lorentzian error norm function, besides Tukey-based operation is taken into account for the decision of CT inserting in each propagation rounds(30 iterations of diffusion).

3) CT inserted time determination. Results of Lorentzian-based and Tukey-based diffusions in a propagating round are compared. A steady region number could remain in an interval in Tukey-based diffusion, but sometimes it will lead to pseudo segmentation due to its sharp stopping. On contrast, Lorentzian-based operation tends to smear boundaries after a certain time. If two reduced region numbers of the two kinds of PDEs vary obviously in a propagation round, it means that region merging is distinct and CT should be taken to avoid weak edges smear.

The halting conditions are also decided by the same analysis. Fig.4 shows the diagram which depicts the judge of CT insertion, Curvelet enhancement and diffusion halting, where $N^{(t)}_{Lorentzian}$, $N^{(t-1)}_{Lorentzian}$, $N^{(t)}_{Tukey}$ and $N^{(t-1)}_{Tukey}$ are partition numbers of Lorentzian-based and Tukey diffusions in iterations *t* and ***t-1***, $f^{(t-1)}_{Lorentzian}$ and $f^{(t-1)}_{Tukey}$ are images before an iteration, while S^{r-1}_{L} is a CT enhanced version of the initial at the start of each round ***r,*** N_L and N_T are changed region numbers used to measure the smear degree of boundaries.

5. EXPERIMENTS AND CONCLUSIONS

To validate the efficiency of our suggested method, we undertook 3 experiments: 1) segmentation surface of the original, 2) partitions of the diffused PDE images with and without CT enhancement, and 3) final result guided by Tukey-based halting condition. Typical results are shown in Fig.5 and Fig.6 with '***dif***'='diffusion', 'CT_i'='***CT*** inserted times'. Images range from high frequencies and low frequencies. All results are obtained by Watershed transform directly on diffusion outputs without any post-processing such as merging or curve evolution. Since the partitioned area is labeled by gray level [0~255], we could observe that the more regions a segmentation result contains, the brighter an image will be, except the original partition of Baboon, for its region number is beyond 256. Fig.5 (b) and (c) have the same diffusion times but without and with CT enhancement, Fig. 5(d) is the final halting result. Similar results are shown in Fig.6, except the stable solution to Peppers arrives earlier because of its smooth content. We could find out:

(1) The suggested approach (Fig.5(c)) is more efficient than typical PDE based method (Fig.5 (b)) when the iteration times are the same, since over-segmentation is greatly improved by diffusion while region smear modified by CT enhancement:

• In the case without CT enhancement (Fig.5 (b)), Baboon's nose is separated into two parts; **furthermore**, part of the nose area is already merged into the area upon lips, thus the full nose region could not be retrieved without special operations. For comparison, the nose area is a complete one in Fig.5(c) where CT is inserted. That means, CT results in large connected regions, which are valuable and preferred in segmentation.

• Besides, many small regions exist in segmentation cases without CT inserted (such as comparisons of Fig.5(b) and (c), refer to the eyes/cheeks/mouth area), over-segmented regions mean harder judgement in post-merging work.

(2) The times of CT insertion depend on image contents. A detail image applies more emphasis to weak edges (Fig.5 (d))

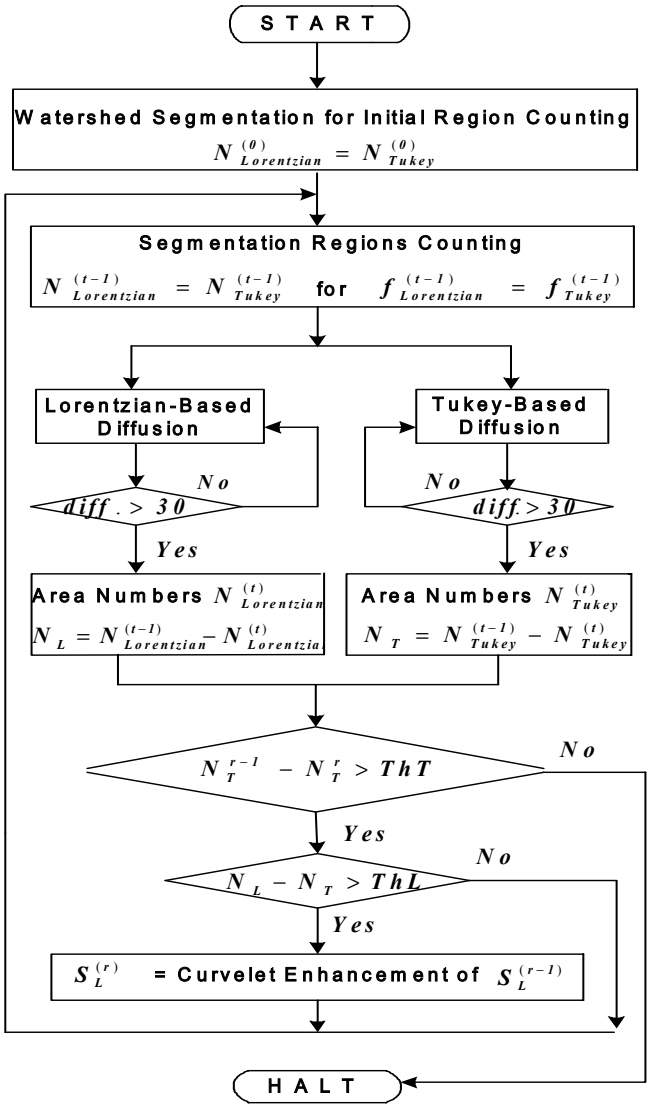

Fig. 4 Diagram of the suggested scheme.

than the one with flat contents (Fig.6 (b)). The first conclusion could be presented clearly in Fig.5 (b) and Fig.5 (c).

We also suggest a criterion to evaluate the segmentation result. It firstly creates a reference signal f^{ref} from Canny edge-map, to extract global object contours by removing local textures in an edge region (shown as Fig.7, Equ (14) and (15)). The segmentation accuracy is calculated finally by summing the boundaries distortion (will be shown as Equ. (16)):

$$f^{ref} = f^{canny} - f^{texture} \tag{14}$$

where

$$f^{texture}(x,y) = \begin{cases} 0, & if \ f^{canny}(x,y) = 0 \\ 1, & f^{canny}(x,y) = 1 \ \&(x,y) in \ texture \end{cases}$$

The above texture block is determined by a quasi-periodic analysis to magnitudes of block signal projections (0^o, 45^o, 90^o, 135^o). For a block of center-line length N, its average projection magnitude is:

$$\mathbf{Mn} = \frac{1}{N}\sum_{m=0}^{N-1} |\, x(m) \,| \tag{15}$$

If the projection signals in 4 directions in a block shows the quasi-period as Fig. 8, the block is viewed as local texture region. Final segmentation accuracy is defined as

$$Segmentation\ \ accuracy = (1 - \frac{\sum f^{ref} \oplus f^{seg}}{\sum f^{ref}}) \times 100\% \qquad (16)$$

where f_{seg} is the final resulted image generated by our method, $\oplus$ denotes an exclusive operation. Fig.9 gives curves of segmentation accuracy comparison, it turns out that by applying diffusion and CT insertion, segmentation accuracy increases. This conclusion is very obvious at the first time CT inserted, especially for the cases of detail image Baboon and noisy Forman. Each time when a CT enhancement performed, the segmentation accuracy steps up, it gains at least 05.% for Lena and 5.2% for noisy Forman in final results, and is at least 1.3% for Peppers and 13.9% for Baboon.

Owing to the multi-scale projections in CT, the suggested approach benefits from CT advantages of region integrity and noise removal. Experiments show clearly that CT enhancement diffusion has a good performance than the conventional PDE-based methods, especially when detail images or weak boundaries are met within objects. CT-based approach does lead to a more balanced segmentation. In addition, it doesn't need initial guesses for object groups and is robust to noise.

6. ACKNOWLEDGMENT

We acknowledge China NNSF(Grant No:60472063) & GDNSF (04020074).

7. REFERENCES

[1] A.Petrovic, O.Escoda,and P.Vandergheynst, "Multireolution Segmentation of Natural Images: From Linear to Nonlinear Scale-Space Representations," *IEEE Trans. Image Process.*, vol.13, No.8, pp. 1169-1186, 2004.

[2] L.Vincent and P.Soille, "Watershed In Digital Spaces: An Efficient Algorithm Based on Immersion Simulations," *IEEE Trans. Patt. Anal. Mach. Intell.*, vol.13, pp. 582-598, Jun. 1991.

[3] S.Thiruven,K.Arcot & Y.Chen,"Pde Bsed Method for Fuzzy Classification of Medical Images"*ICIP2006*,pp.1805-1808,2006

[4] A.Tsai etc.,"Curve evolution implementation of Mumford-Shah functional for segmentation, denoising, interpolation and magnifi."*IEEE Trans.Image Process.*,vol.10,No.8,pp.1169-1186,2001

[5] Z. Le, "Digital Image Information Processing," *National Defence Industry Press*, 2003.

[6] J-L. Starck, F. Martagh, E. J. Candès, and D. L. Donoho, "Gray and Color Image Contract Enhancement by Curvelet Transform",*IEEE Trans.Image Process.*,vol.12,N0.6,pp.706-717, 2003.

[7] P.Perona and J.Malik,"Scale-Space & Edge Detection Using Anisotropic Diff.",*IEEE Trans.PAMI.*,vol.12,N0.7,pp629-639,1990.

[8] M.J.Black,G.Sapiro,D.H.Marimont,D.Heeger,"Robust Anisotropic Diff-usion," *IEEE Trans. On Image Processing*, vol.7, No.3, pp421-432,1998

[9] A.Ben Hamza, H. Krim and G.B. Unal, "Unifying Probabilistic and Variational Estimation," IEEE Signal Processing Magazine, Vol.19,No. 5, pp.37 – 47, 2002

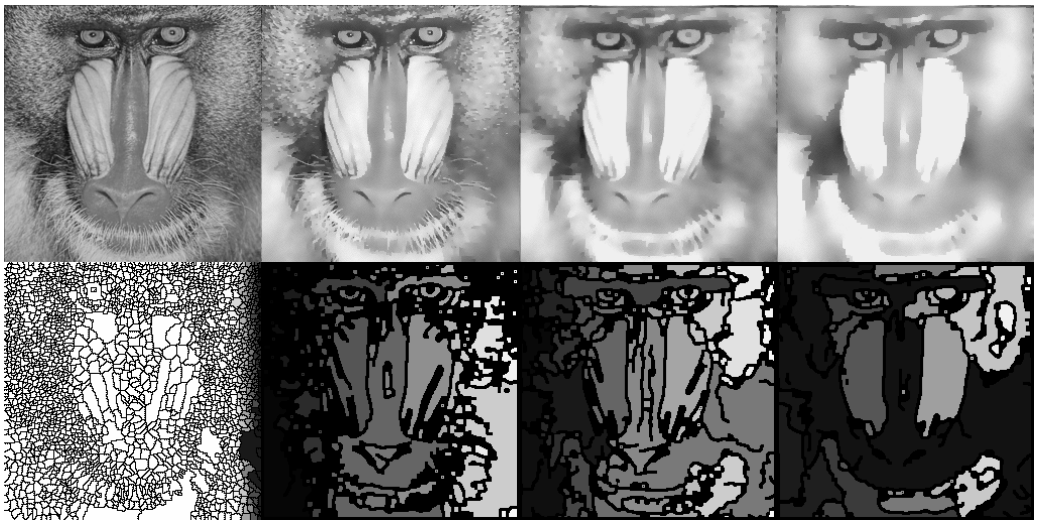

(a)original (b)*dif*=30,*CTi*=0 (c)*dif*=30,*CTi*=1 (d)*dif*=90,*CTi*=3

Fig.5 Diffusion and segmentation on Baboon without merging

Fig.7 Reference maps

(a)dif=30,CTi=0 (b)dif=30,CTi=1 (c)dif=90,CTi=2 (d)dif=90,CTi=3

Fig. 6 Diffusion and segmentations on Peppers/Lena/noisy Forman.

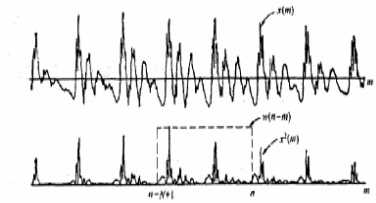

Fig.8 Texture projection

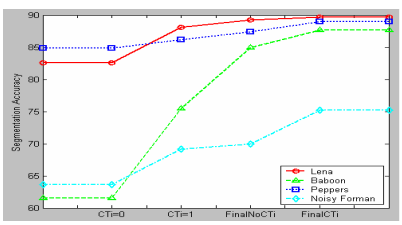

Fig.9 Segmentation performance